

<b>Customer</b>	: ESTEC	<b>Document Ref</b>	: FRM4SST-CR-DMI-001
<b>Contract No</b>	: 3-15990/19/NL/IA	<b>Issue Date</b>	: 12 February 2021
<b>WP No</b>	: 70	<b>Issue</b>	: 1

**Project** : FRM4SST (ships4sst)

**Title** : Characterisation Report

**Abstract** : This document contains the Characterisation report for C-band radiometer, including results from pilot inter-comparison on the FRM4SST Service.

**Author(s)** : Jacob L. Høyer\*, Sotirios Skarpalezos\*, Sten S. Søbjerg<sup>‡</sup>

\_\_\_\_\_

Project Scientist

\*DMI

‡DTU

**Approved by** :



\_\_\_\_\_

Ruth Wilson  
Project Manager  
Space ConneXions Limited

**Accepted by** :

\_\_\_\_\_

Craig Donlon  
ESA Technical Officer  
ESTEC

**Distribution** : FRM4SST Project Team  
ESA

**EUROPEAN SPACE AGENCY  
CONTRACT REPORT**

The work described in this report was done under ESA contract.  
Responsibility for the contents resides in the author or organisation  
that prepared it.

## **AMENDMENT RECORD**

This document shall be amended by releasing a new edition of the document in its entirety. The Amendment Record Sheet below records the history and issue status of this document.

### **AMENDMENT RECORD SHEET**

<b>ISSUE</b>	<b>DATE</b>	<b>REASON FOR CHANGE</b>
A	29/01/2021	Draft for first internal review
B	11/02/2021	Updated following feedback
1	12/02/2021	Issued to ESA

## TABLE OF CONTENTS

<b>1. INTRODUCTION</b>	<b>4</b>
<b>2. REFURBISHMENT OF EXISTING HARDWARE AND NEW DESIGN</b>	<b>5</b>
2.1 Existing hardware	5
2.2 Top level design of new sensors	6
2.3 Antenna design	8
2.4 Sensor implementation	11
2.5 Physical specifications	11
2.6 Software resources	12
<b>3. CALIBRATION STRATEGY</b>	<b>14</b>
3.1 Internal calibration	14
3.2 Correction for transmission lines	15
3.3 Correction for antenna parameters	16
3.4 Other corrections	18
<b>4. CHARACTERIZATION OF NEW RADIOMETERS</b>	<b>20</b>
4.1 Characterization of gain, noise temperature	20
4.2 Calibration of internal calibration point, Noise Diode	22
4.3 Characterization of antenna system parameters	25
4.4 Long term stability	28
<b>5. PREPARATION FOR TEST CAMPAIGN</b>	<b>32</b>
5.1 System setup and operation plan	32
<b>6. SHORT-TERM MEASUREMENT CAMPAIGN</b>	<b>34</b>
6.1 Campaign site and setup	34
6.2 Brief description of the infrared radiometer	34
6.3 Qualitative description of experiment conditions	34
6.4 Results	35
<b>7. SUMMARY AND CONCLUSIONS</b>	<b>38</b>
7.1 Main characteristics	38
7.2 Conclusions	39
<b>8. REFERENCES</b>	<b>41</b>

## **1. INTRODUCTION**

This document describes the refurbishment of two radiometers owned and operated by DTU-Space with preliminary results from a static Infrared and Microwave radiometer inter-comparison pilot campaign. The existing Microwave instruments are designed for different types of operations, and no instrument exists for measurements at the CIMR C-band frequency, 7.0 GHz  $\pm$ 100 MHz.

Complete design of two sensors from scratch would require a significant budget for components, data collection and data storage hardware, support structures, mechanical and thermal housing, and a substantial amount of man power would be required in order to design, implement, and test all elements. Hence, the instruments would be expected to be ready no earlier than 1.5 – 2 years from kick-off.

With the use of existing sensors, all data collection hardware, data storage hardware, support structures, power supplies, mechanical and thermal housing can be reused, and hence the upgrade would only have to focus on the receiver front end, adapting to the upgraded frequency requirements. This upgrade includes receiver chains, but it also includes calibration references and the necessary support for application of a suitable calibration strategy.

Chapter 2 of the document identifies possible donor instruments to be refurbished, and it describes the actual redesign and implementation, including required software resources. Chapter 3 outlines the calibration strategy, and chapter 4 applies the strategy in order to characterize all relevant parts of the instrument, including the important built-in calibration points. In chapter 5 the proposed setup for a short, supervised test and demonstration campaign is presented, and finally, chapter 6 gives a short summary and conclusions.

## 2. REFURBISHMENT OF EXISTING HARDWARE AND NEW DESIGN

This chapter describes the preparation of the sensors EMIRAD-C and EMIRAD-X for radiometric measurements in the frequency bands at 7.05 GHz and 10.69 GHz, respectively. The sensors are based on refurbishment of existing hardware, operated and owned by DTU-Space, and the subsections will demonstrate the process of transformation.

### 2.1 Existing hardware

For the preparation of the two new sensors, several existing instruments are available:

- L-band: 2 versions of EMIRAD-L, 1400-1427 MHz, full Stokes
- C-band: Very old C-band radiometer, 4.8-5.0 GHz, Single H or V channel – Data collection NOT WORKING, and several components outdated
- X-band: Test bed for stability measurements, 10.64-10.74 GHz, 2 inputs measured in time multiplex. Calibration system not ready for field measurements, and no antenna exists
- Ku-band: EMIRAD-Ku, 16.1-16.5 GHz, full Stokes
- Ka-band: EMIRAD-Ka, 34.1-34.5 GHz, full Stokes

All instruments are built as modular systems with discrete building blocks, which can be individually replaced or upgraded. Typical building blocks are “analog front end” (AFE), “digital front end” (DFE), “system control unit” (SCU), and “power supply” unit (PSU). Figure 2-1 shows typical radiometer designs for L-and Ka-band, respectively.

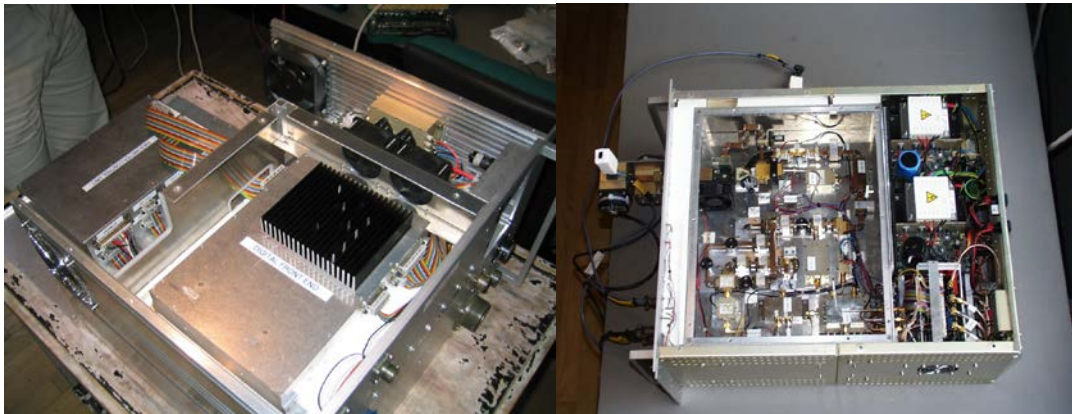


Figure 2-1 – EMIRAD-L and EMIRAD-Ka, Examples of modular design

The outdated C-band radiometer is in a very bad condition, and it is considered extremely manpower and component consuming to get it up to present standard. The Ku-/Ka- band sensors are equipped with 25-year-old data collection systems, and it is considered high risk to rely on this hardware. As the data collection system is one of the most time-consuming

elements to upgrade, this is not a feasible way. As two almost identical versions exist of the L-band sensor, and as this instrument is equipped with the most modern data collection and data handling system, it is a good choice for a C-band sensor. The most severe limitation is the bandwidth, but as the target is very slowly varying, and plenty of integration time is available for the foreseen activities, the lack of bandwidth is easily compensated through integration. As a benefit, the instrument is fully polarimetric and it thus measures two polarizations along with the 3<sup>rd</sup> and 4<sup>th</sup> Stokes parameters in parallel. For the X-band sensor it is very attractive to build upon the existing X-band radiometer, updating only the calibration facility and designing an antenna system. This instrument also features a modern data collection system. Hence it has been decided to upgrade the existing X-band system, while reconfiguring one of the L-band sensors to measure the C-band.

A rough schematic of a typical radiometer design is shown in Figure 2-2. It is seen that the microwave section is encapsulated in a double layer of insulation in order to keep a stable operating temperature. Furthermore, the system control unit includes a regulation feedback loop in order to maintain the desired temperature.

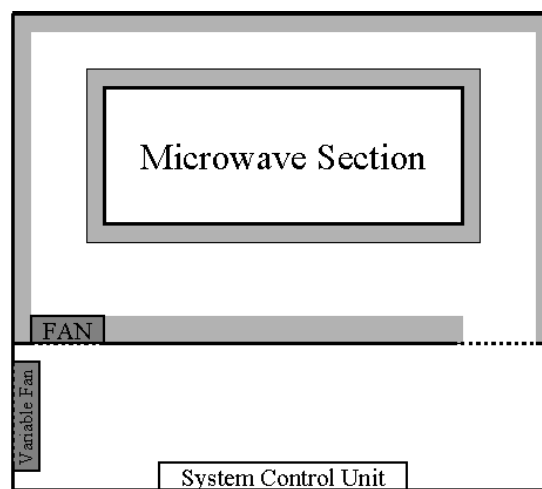


Figure 2-2 – Schematic showing the layout of a typical radiometer

## 2.2 Top level design of new sensors

The C-band sensor needs the most severe upgrade. A completely new front-end has to be implemented, receiving the desired frequency band and subsequently down-converting it to the existing L-band. This add-on also calls for a new noise injection calibration point, as this feature has to be located as close to the instrument input as possible in order to include all components in the calibration loop. The result is outlined in Figure 2-3, where components shown in red are new additions, and where components in green are existing components, which have to be replaced in order to comply with the frequency requirement. Only components in white can be reused as is. Small attenuators have been added in order to fine-tune the overall gain, and in order to avoid saturation of amplifiers in the back-end of the receiver chain. Furthermore, the attenuators improve component matching and reduce standing waves.

For the X-band instrument, the upgrade includes the noise injection facility up front and a completely new design of an antenna system. The block diagram is seen in Figure 2-4, where the red/green colour coding has been applied similar to the C-band diagram.

As illustrated in the figures, both designs call for a new antenna system along with the addition of several components.

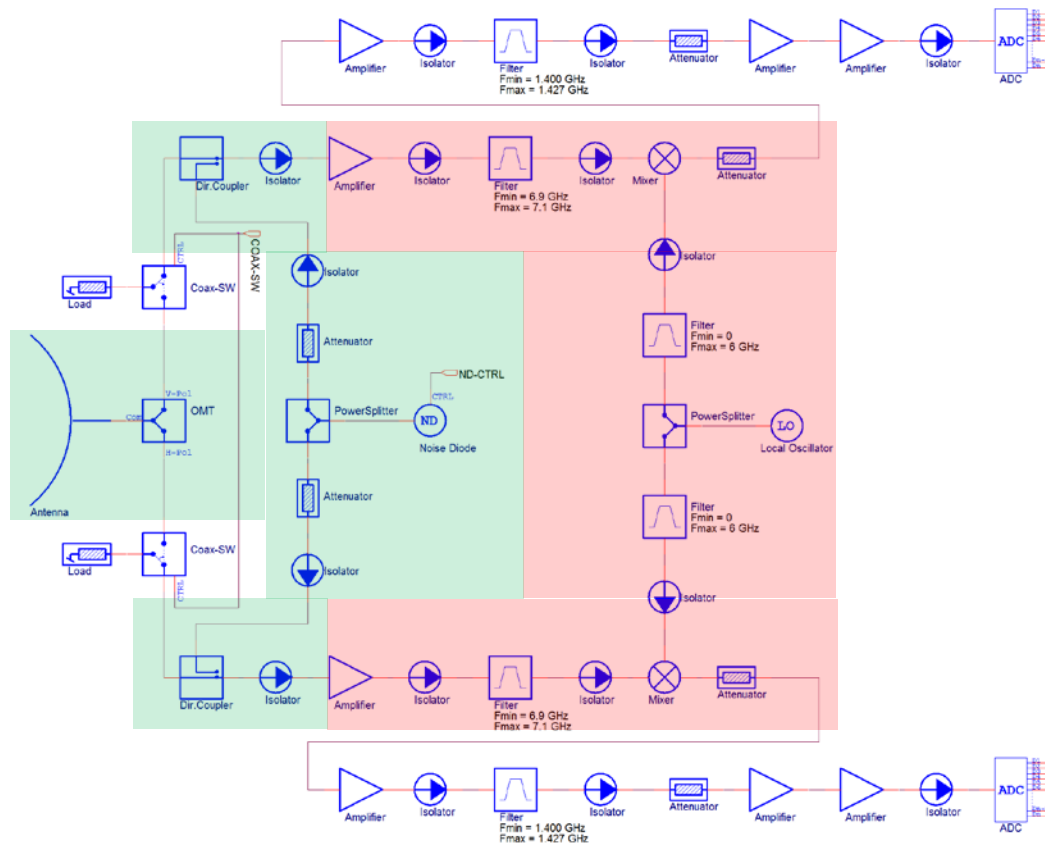


Figure 2-3 – Block diagram for EMIRAD-C. Components without shadow could be reused, while components in green shadow had to be replaced in order to cope with the new frequency. All components in red shadow are new additions, which were not part of the donor instrument.

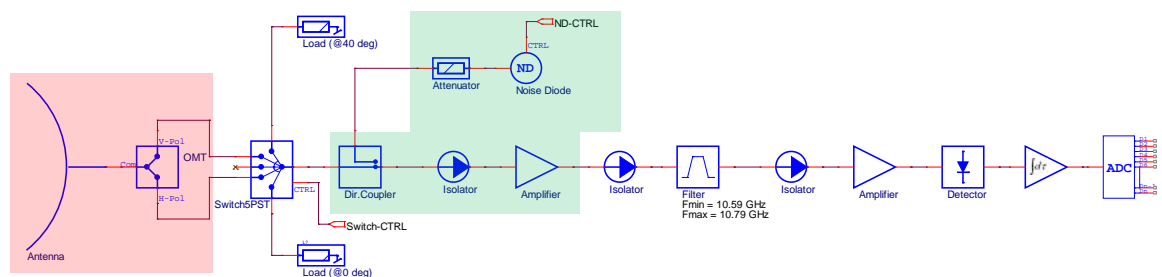


Figure 2-4 – Block diagram for EMIRAD-X. Components without shadow could be reused, while components in green shadow had to be replaced in order to cope with the new frequency. All components in red shadow are new additions, which were not part of the donor instrument.

## 2.3 Antenna design

The antennas designed for the project are horn antennas, as they feature a very low loss, which is a key feature for well calibrated radiometer measurements. As the instruments are required to measure at two orthogonal polarizations, either two individual horns are required, or the design needs to aim at a square shaped or a circular horn. As the C-band instrument is designed to measure the full Stokes vector, and as this would be an attractive add-on to the X-band sensor in the future as well, the two-antenna solution is not feasible, as the antennas need to have a common phase centre in order to obtain the 3<sup>rd</sup> and 4<sup>th</sup> Stokes parameters through correlation of the two orthogonal polarizations [4]. As the manufacturing of circular horns is much more time consuming than for a square shaped horn, the latter is chosen in order to comply with the project time schedule.

From [1], typical radiation patterns for rectangular and square shaped horns can be found. The patterns are shown in Figure 2-5. The parameter for the horizontal axis is given as a function of the physical length and width of the aperture, A and B, respectively, and where  $\lambda$  represents the wavelength. The curve parameter, s, is found from the equations given in the Figure, where Rh and Re represent the side length from the antenna feed point to the aperture for the E- and H-plane respectively. For a single polarized antenna, the rectangular shape is attractive, as it allows for equal width in the E- and H-planes, but as this project requires both polarizations to be measured, the square shape must be chosen as a compromise.

For both planes it is seen that for values of s up to 0.3 the curves change relatively little, while going beyond 0.3 significantly compromises the radiation pattern. To avoid excessive horn depth, 0.3 is chosen as the best possible compromise. The aperture size, i.e. the values A and B (which are equal for a square shape), defines the antenna gain and thus the half-power beam width. A typical radiometer antenna would aim for 20-25 dB gain, but for 25 dB gain the C-band horn would have to be D = 900 mm deep in order to keep s = 0.3. Backing off to 24 dB reduces the depth to D = 700 mm, which is considered fair in order to keep mechanical installation challenges at a reasonable level, as the mass of the antenna as well as the wind pressure on it will increase by  $D^2$ . Thus the required support structure will have to be scaled up accordingly, and eventually it may be difficult or even impossible to fit it onto a bridge or a ship.

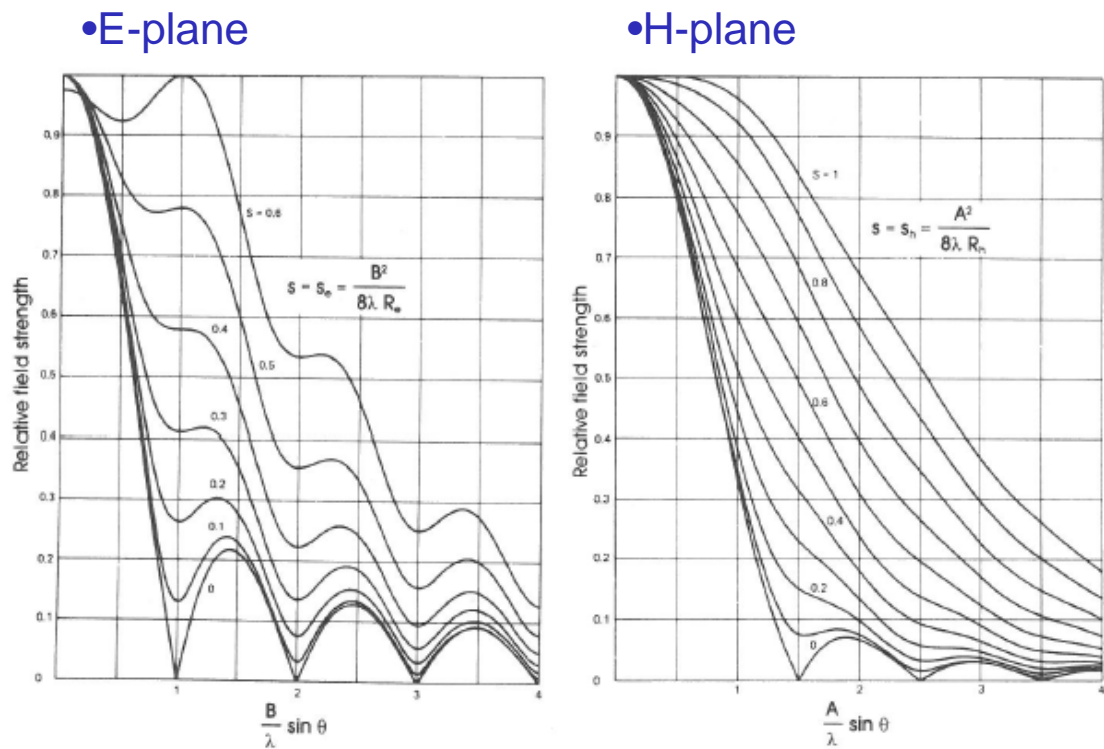


Figure 2-5 – Antenna radiation pattern for a rectangular or square shaped antenna [1]

With 24 dB gain, the side length for the C-band aperture will be 274 mm, while the X-band antenna will be 180 mm. The depths are 700 mm and 460 mm respectively. With the chosen values, the scaling of the horizontal axis will be as shown in Table 2-1, allowing data users to evaluate the beam efficiency and compute the incidence angle span. As both antennas have the same design parameters, the scaling for the C-band horn and the X-band horn is the same.

$L/\lambda \cdot \sin(\Theta)$	E-plane	H-plane
1	9.0 deg.	9.0 deg.
2	18.3 deg.	18.3 deg.
3	28.0 deg.	28.0 deg.
4	38.8 deg.	38.8 deg.

Table 2-1 – Scaling of the horizontal axis for antenna horn radiation patterns shown in Figure 2-1, using the dimensions chosen for the EMIRAD-C and EMIRAD-X antenna horns

At the horn output both antennas must be equipped with an Ortho Mode Transducer (OMT) in order to allow the signals from the two polarizations to be output on independent connector ports. The OMTs for both bands are available from third-party component manufacturers. The

complete antenna system for C-band and X-band is shown in Figure 2-6 and Figure 2-7, respectively.

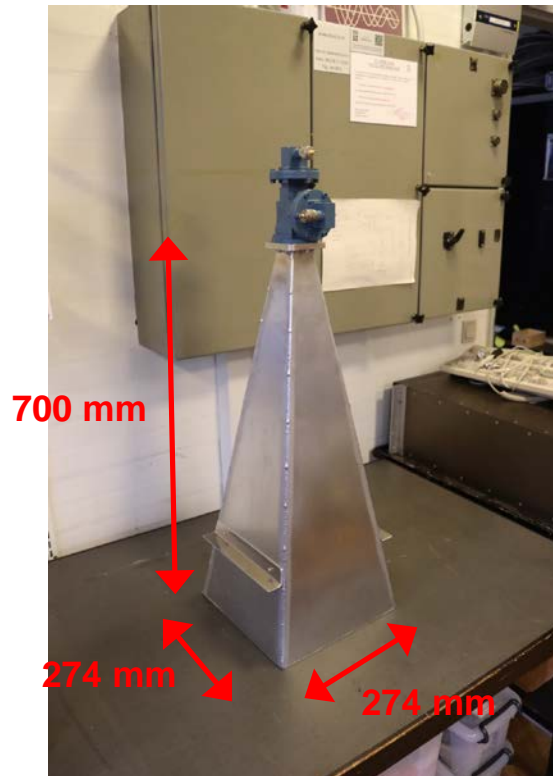


Figure 2-6 – Complete antenna system, including Ortho Mode Transducer, for C-band

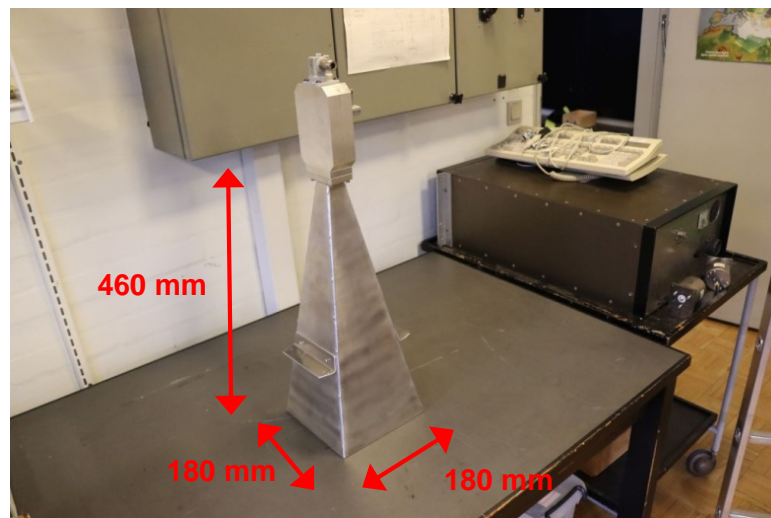


Figure 2-7 – Complete antenna system, including Ortho Mode Transducer, for X-band

## 2.4 Sensor implementation

The two sensors are upgraded according to Figure 2-3 and Figure 2-4, respectively. As it is seen in Figure 2-3, the C-band radiometer needs several additional components, while others must be replaced. Figure 2-8 shows the process, where the left picture shows the instrument when only reusable components are left in place, and where the right picture shows, how the additional components are added as an extra layer above the existing component plate. After the picture was taken, cables and electrical connections were added, before the box was closed.



**Figure 2-8 – The refurbishment of EMIRAD-C. Left: only reusable components are left in the analogue front-end box. Right: Additional components have been fitted on a separate component layer, mounted on top of the existing component plate**

The two completed radiometers are shown in Figure 2-9, with EMIRAD-C in the left picture and EMIRAD-X in the right picture. Not shown is a third box containing the power supplies for EMIRAD-C, which has to be accommodated separately less than 4 m from the radiometer. Power supply is included in EMIRAD-X.



**Figure 2-9 – The completed EMIRAD-C (left) and EMIRAD-X (right)**

## 2.5 Physical specifications

Key features for EMIRAD-C are:

Measures: 316 mm x 346 mm x 333 mm (including box fixed to the top)

Measures: 428 mm x 410 mm x 141 mm (Power supply box)

Mass: 19 kg (radiometer) + 15.5 kg (Power supply)

Power consumption: 1.15 A @230 VAC = 264,5 W (max)

Key features for EMIRAD-X are:

Measures: 428 mm x 465 mm x 225 mm

Mass: 28.5 kg

Power consumption: 0.87 A @230 VAC = 200 W (max)

## 2.6 Software resources

Both radiometer systems come with a graphical user interface (GUI) for easy setup, operation and monitoring. The two applications can run on the same computer, which must feature a Windows environment. When the instruments are operated, the GUI can be used to monitor the measured data continuously, or the GUI may be closed. Data from the radiometers is stored via an FTP (File Transfer Protocol) connection to any computer visible on the network, identified through its IP-number. The IP-number can be configured through the GUI, and it may/may not be the same computer used for instrument control. For a short, supervised campaign, it may be favourable to use the same computer, while a longer campaign might have a central storage facility, independent from the GUI, which is typically closed, when the operator is not present. The two GUIs are seen in Figure 2-10, with EMIRAD-C to the left and EMIRAD-X to the right.

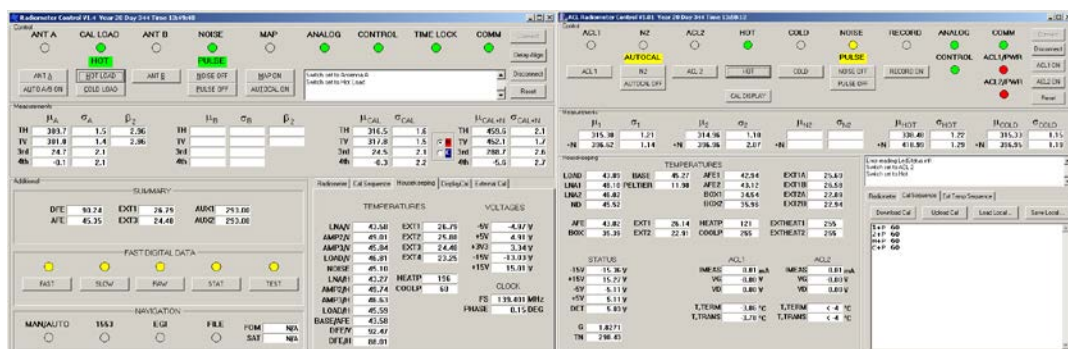


Figure 2-10 – User interface for EMIRAD-C (left) and EMIRAD-X (right)

Data is recorded in a binary format for compression and efficient use of storage capacity. EMIRAD-C has a basic integration time equal to  $\tau = 1$  ms, and it outputs two files every 30 seconds with a total data rate of 248 MB/hour. For EMIRAD-X the basic integration time equals  $\tau = 8$  ms, and it outputs one file every 2 minutes with a total data rate of 55 MB/hour.

After completion of the measurement, data is converted into a set of ASCII-files using the applications "Unpack2.exe" and "ACLUnpack.exe" for EMIRAD-C and EMIRAD-X, respectively. Further processing includes synchronization of measurement data and housekeeping data, integration to user defined observation times, computation of calibration coefficients, application of actual calibration, and correction for external parameters (see chapter on calibration strategy). This is done by the applications "Intcal.exe" and "Intcal-X.exe", respectively. The final data product is one (EMIRAD-C) or two (EMIRAD-X) ASCII text files with numbers organized in columns, where data content is:

Column 1: Time (s, Unix time)

Column 2: V-pol data (K)

Column 3: H-pol data (K)

Column 4: 3<sup>rd</sup> Stokes data (K, only EMIRAD-C)

Column 5: 4<sup>th</sup> Stokes data (K, only EMIRAD-C)

Columns 6-7: Housekeeping data

Column 8-23: Internal temperatures

Column 24-33: Reserved for navigation data for a campaign on a moving platform

### 3. CALIBRATION STRATEGY

The calibration scheme for both instruments follows the same principle as the existing EMIRAD-L, which is described in [2] and [3]. Basically, it is a four-step procedure, where the first step uses the internal calibration references to calibrate up to a calibration reference equal to the instrument front plate. Step two considers the transmission lines between the antenna system and the radiometer, and step 3 accounts for the antenna system itself. Finally, step 4 accounts for the actual antenna orientation with respect to Earth North and true Horizontal/Vertical orientation. The four steps are shown in Figure 3-1.

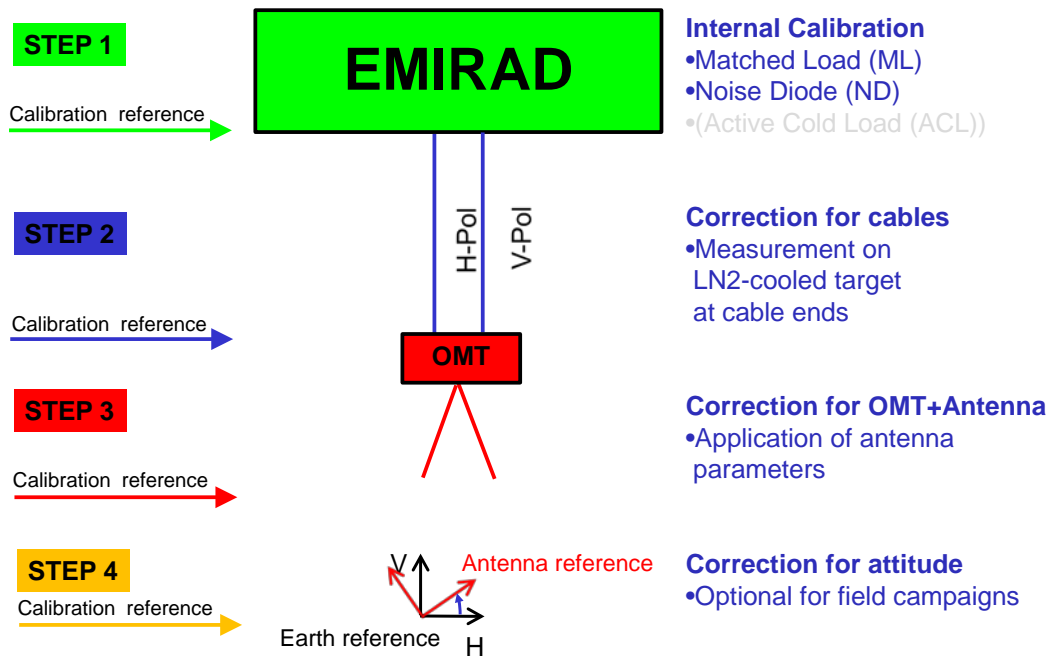


Figure 3-1 – Calibration steps for EMIRAD-C and EMIRAD-X

#### 3.1 Internal calibration

Step 1 (shown in green in Figure 3-1) in the calibration process is translation from digital counts to brightness temperatures at the instrument input, as it is shown in Figure 3-2.

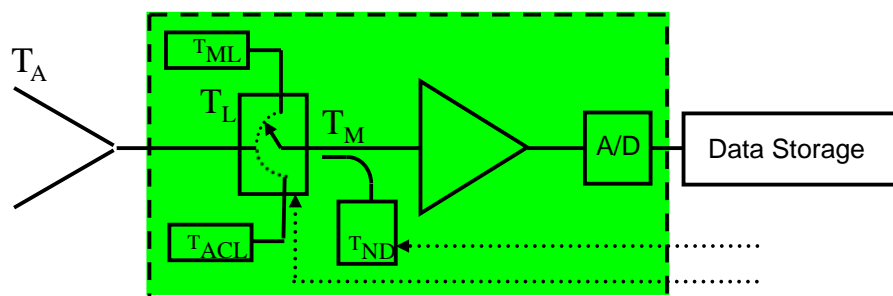


Figure 3-2 – Internal calibration based on a matched load and a noise diode

The Matched Load, ML, outputs a brightness, which is equal to its physical temperature, which is continuously monitored. It is the simplest calibration target, and it is sometimes referred to as “hot load”. A mechanical switch switches between the antenna input and the reference. At this point a so-called active cold load (ACL) could be applied according to [3], but it is currently not implemented in the two instruments. However, room is reserved for ACLs, and the switches support it. In the current setup a Noise diode, ND, (constant current diode) acts as second calibration point, as these devices are known to be extremely stable over time. The noise diode adds a well known (after characterization) amount of noise on top of whatever brightness is being measured. Thus, the instrument gain is directly determined, while the matched load along with the gain determines the noise temperature, i.e. a full two-point calibration. The only action required to make the procedure operational is characterization of the noise diode as a function of operational temperature (see chapter on characterization). The calibration components along with the flexible instrument control through the GUIs allow for operation as Total Power Radiometer (TPR), quasi Dicke Radiometer (DR) or quasi Noise Injection Radiometer (NIR), dependent upon the actual configuration settings.

### 3.2 Correction for transmission lines

Transmission lines contribute significantly to the measured brightness temperature at microwave frequencies. According to [4], the observed Brightness Temperature,  $T_A'$  is found from

$$T_A' = GT_A + (1 - G)T_P \quad (3-1)$$

where G is the Gain (<1) of the transmission line,  $T_A$  is the input antenna temperature, and  $T_P$  is the physical temperature of the transmission line, which is constantly monitored. Rearrangement of the equation yields

$$T_A = \frac{T_A' - (1 - G)T_P}{G} \quad (3-2)$$

providing the true brightness temperature at the input to the transmission line based upon the observed brightness temperature after step 1,  $T_A'$ . To make the step (calibration step 2, shown in blue in Figure 3-1) operational, the Gain (Loss factor) for each individual transmission line must be characterized (see chapter on characterization), and a well-known brightness temperature (different from the transmission line physical temperature) at the cable input is required. For the latter, e.g. a liquid Nitrogen cooled matched load in a cryostat, see Figure 3-3, can be used.



Figure 3-3 – Cryostat containing a matched load

The typical application of the cryostat is seen in Figure 3-4. Knowing the factor G for each cable allows the post processing to apply equation

$$T_A = \frac{T'_A - (1 - G)T_P}{G}$$

(3-2) to each data entry.



Figure 3-4 – Application of liquid Nitrogen cooled matched load in cryostat during a field campaign.

### 3.3 Correction for antenna parameters

Following the signal path from the radiometer, the antenna system, i.e. the horn including the Ortho Mode Transducer (OMT), is the final building block to include in the calibration process. This is calibration step 3 (shown in red in Figure 3-1). Several possible artefacts have to be accounted for: insertion loss, return loss, phase imbalance, and cross coupling. Insertion loss is similar to the G-factor for the transmission lines, and it is accounted for using Equation

$$T_A = \frac{T'_A - (1 - G)T_P}{G} \quad (3-2).$$

Return loss almost introduces the same distortion as insertion loss. It occurs due to mismatch between transmission lines or between the antenna and free space. Return loss describes the fraction of the incident signal, which is rejected by the antenna, and it is given by the parameter  $S_{22}$ . Return loss also means that a fraction of the noise generated by the radiometer itself is added on top of the signal, and according to [4] and [5], the total signal received can be described by Equation

$$T'_A = (1 - S_{22})T_A + S_{22}T_N \quad (3-3),$$

where  $T_N$  is the noise temperature, radiated by the radiometer (physical temperature if the input features an isolator as EMIRAD does, or the system noise otherwise), and  $T_A$  is the true antenna temperature.

$$T'_A = (1 - S_{22})T_A + S_{22}T_N \quad (3-3)$$

Inversion of Equation  $T'_A = (1 - S_{22})T_A + S_{22}T_N$

$$T_A = \frac{T'_A - S_{22}T_N}{(1 - S_{22})}$$

(3-3) yields Equation

(3-4), which returns the true antenna temperature.

$$T_A = \frac{T'_A - S_{22}T_N}{(1 - S_{22})} \quad (3-4)$$

A third effect introduced by the antenna system is phase imbalance, which causes a mixing of the 3<sup>rd</sup> and 4<sup>th</sup> Stokes parameters. The situation is illustrated in Figure 3-5, and the correction

is seen in Equation  $\overline{T}_B = \begin{pmatrix} I \\ Q \\ U \\ V \end{pmatrix} = \begin{pmatrix} 1 & 0 & 0 & 0 \\ 0 & 1 & 0 & 0 \\ 0 & 0 & \cos(\varphi) & -\sin(\varphi) \\ 0 & 0 & \sin(\varphi) & \cos(\varphi) \end{pmatrix} \begin{pmatrix} I' \\ Q' \\ U' \\ V' \end{pmatrix}$  (3-5), which outputs the

correct Stokes Vector (I, Q, U, V) based on the observed Stokes vector (I', Q', U', V'), where  $\varphi$  is the phase error.

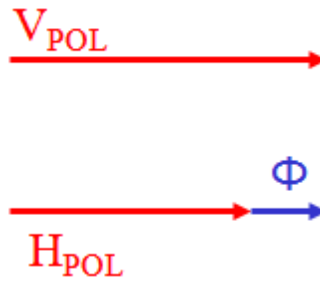


Figure 3-5 – Path length difference between channels introduce a phase error

$$\overline{T}_B = \begin{pmatrix} I \\ Q \\ U \\ V \end{pmatrix} = \begin{pmatrix} 1 & 0 & 0 & 0 \\ 0 & 1 & 0 & 0 \\ 0 & 0 & \cos(\varphi) & -\sin(\varphi) \\ 0 & 0 & \sin(\varphi) & \cos(\varphi) \end{pmatrix} \begin{pmatrix} I' \\ Q' \\ U' \\ V' \end{pmatrix} \quad (3-5)$$

The final correction to the antenna system deals with possible cross coupling, illustrated in Figure 3-6. The coupling coefficient  $\rho$  introduces a mixing of the 2<sup>nd</sup> and the 4<sup>th</sup> Stokes parameters, according to [5], and for correction Equation

$$\overline{T}_B = \begin{pmatrix} I \\ Q \\ U \\ V \end{pmatrix} = \begin{pmatrix} 1 & 0 & 0 & 0 \\ 0 & 1-2\rho & 0 & -2\sqrt{\rho-\rho^2} \\ 0 & 0 & 1 & 0 \\ 0 & 2\sqrt{\rho-\rho^2} & 0 & 1-2\rho \end{pmatrix} \begin{pmatrix} I' \\ Q' \\ U' \\ V' \end{pmatrix} \quad (3-6)$$

is applied. Again, the

correct Stokes Vector is (I, Q, U, V), while the observed Stokes vector is (I', Q', U', V').

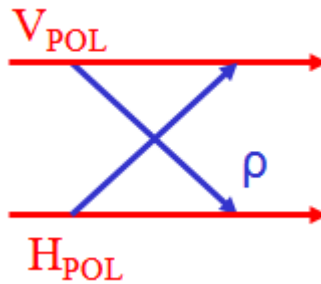


Figure 3-6 – Cross coupling between channels in the antenna system.

$$\overline{T}_B = \begin{pmatrix} I \\ Q \\ U \\ V \end{pmatrix} = \begin{pmatrix} 1 & 0 & 0 & 0 \\ 0 & 1-2\rho & 0 & -2\sqrt{\rho-\rho^2} \\ 0 & 0 & 1 & 0 \\ 0 & 2\sqrt{\rho-\rho^2} & 0 & 1-2\rho \end{pmatrix} \begin{pmatrix} I' \\ Q' \\ U' \\ V' \end{pmatrix} \quad (3-6)$$

### 3.4 Other corrections

Although calibration steps 1-3 account for all instrument related effects, a fourth step (shown in yellow in Figure 3-1) is required and included in the software package. The artefact is introduced, if the physical installation of the antenna system is rotated by the angle  $\theta$  with respect to true horizontal and vertical polarizations at the Earth surface. The situation is illustrated in Figure 3-7, and the result is a mixing of the 2<sup>nd</sup> and 3<sup>rd</sup> Stokes parameters. Knowing the rotation angle allows for correction, using Equation

$$\overline{T}_B = \begin{pmatrix} I \\ Q \\ U \\ V \end{pmatrix} = \begin{pmatrix} 1 & 0 & 0 & 0 \\ 0 & \cos(2\theta) & -\sin(2\theta) & 0 \\ 0 & \sin(2\theta) & \cos(2\theta) & 0 \\ 0 & 0 & 0 & 1 \end{pmatrix} \begin{pmatrix} I' \\ Q' \\ U' \\ V' \end{pmatrix} \quad (3-7)$$

Figure 3-1 – Calibration steps for EMIRAD-C and EMIRAD-X, which is found in [2] and [4].

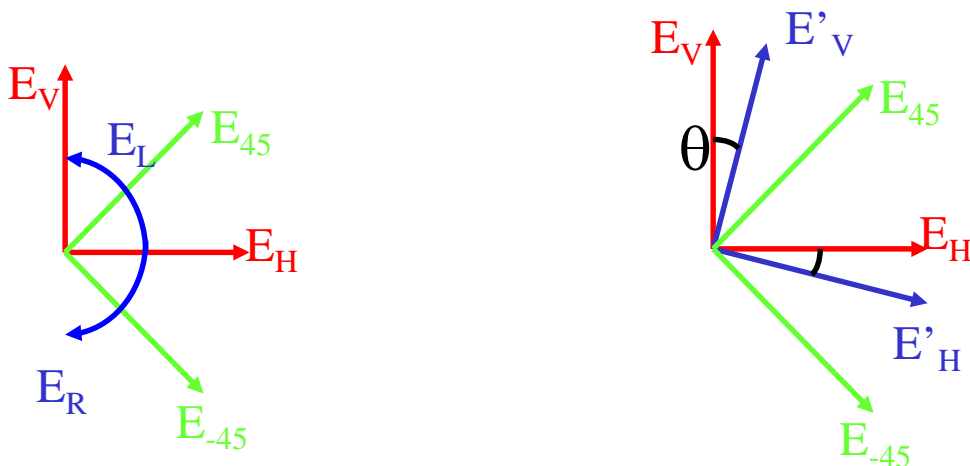


**Figure 3-7 – The polarizations required for measurement of the full Stokes vector (left), and the resulting observed Stokes vector (right), if the antenna system is rotated with respect to true Horizontal and Vertical polarization.**

$$\overline{T}_B = \begin{pmatrix} I \\ Q \\ U \\ V \end{pmatrix} = \begin{pmatrix} 1 & 0 & 0 & 0 \\ 0 & \cos(2\theta) & -\sin(2\theta) & 0 \\ 0 & \sin(2\theta) & \cos(2\theta) & 0 \\ 0 & 0 & 0 & 1 \end{pmatrix} \begin{pmatrix} I' \\ Q' \\ U' \\ V' \end{pmatrix} \quad (3-7)$$

Unlike calibration steps 1-3, calibration step 4 is not necessary in a stationary campaign, if the antenna system is carefully installed. However, for a moving platform, e.g. an aircraft or a ship, the platform attitude must be measured continuously and time synchronized to the radiometer data for proper data processing.

## 4. CHARACTERIZATION OF NEW RADIOMETERS

Knowing the instrument architecture and the calibration strategy for EMIRAD-C and EMIRAD-X, the requirements for characterization can be set up. The internal load and the internal noise diode will provide two calibration points, if they are well known. The matched load just needs a temperature measurement, but the noise diode must be characterized prior to application as calibration target. Also, the external characteristics of transmission lines and antenna system must be estimated. In total a full characterization includes

- Determination of noise diode contribution as a function of its physical temperature
- Validation of linearity (to allow for calibration based on the noise diode)
- Measurements of transmission line losses (insertion loss)
- Measurement of antenna system insertion loss
- Measurement of antenna system return loss
- Measurement of antenna system phase imbalance
- Measurement of antenna system cross coupling

### 4.1 Characterization of gain, noise temperature

To determine the contribution from the noise diode, it is necessary to first determine the absolute instrument gain and noise temperature. Since only the matched load provides a known internal calibration point (as long as the noise diode is unknown), an external calibration point is required. Here the liquid Nitrogen cooled match load in the cryostat is useful, as it can be directly attached to the radiometer inputs as illustrated in Figure 4-1.

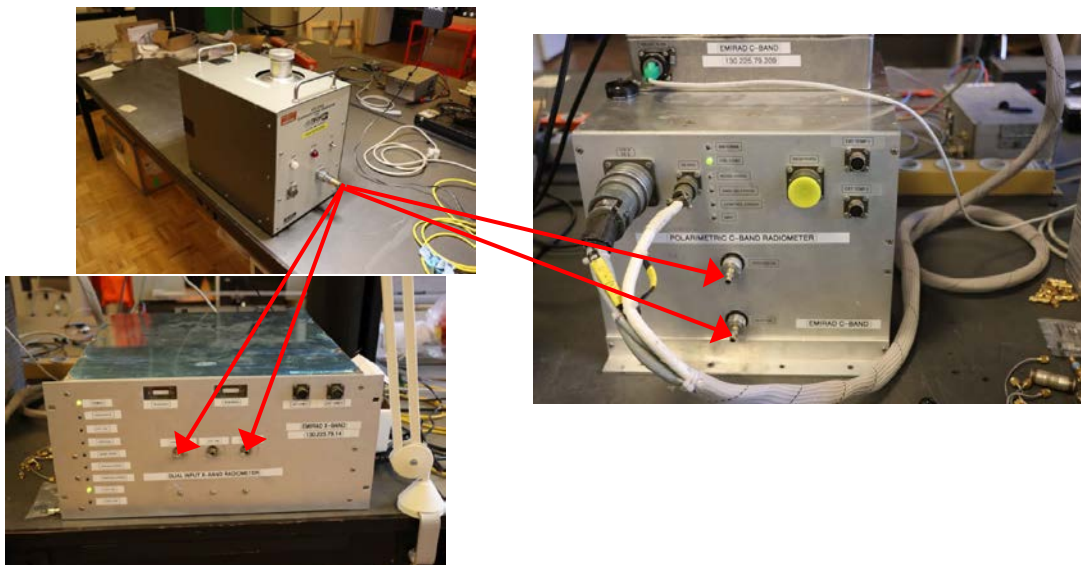


**Figure 4-1 – Liquid Nitrogen cooled matched load is connected directly to each radiometer input for accurate two-point calibration**

The test is repeated several times for different settings of the internal temperature regulation system. The purpose is to determine not only a mean value for the noise diode but to characterize it over a reasonable temperature span in order to enable data calibration independent from the actual temperature setting. Each temperature setting results in an individual estimate for the system gain and the system noise temperature, shown in Figure 4-2 and Figure 4-3 for EMIRAD-C and EMIRAD-X, respectively. Trend lines have been added to all figures in order to estimate the sensitivity to temperature variations. However, it is important to note that these trend lines are not part of the calibration strategy, as actual values for gains and noise temperatures are re-calculated on an ongoing basis, following the regular calibration events.

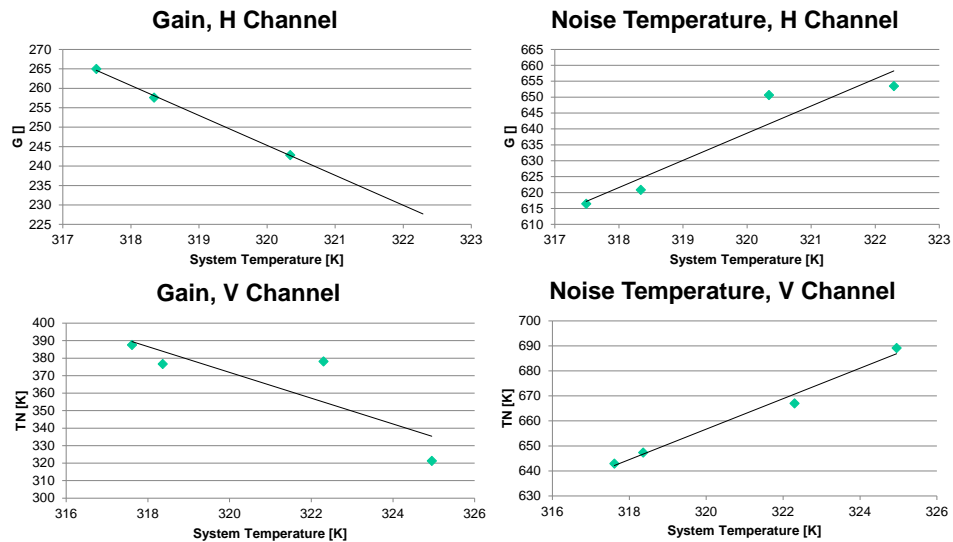


Figure 4-2 – Gain and noise temperature estimates for EMIRAD-C determined as a function of internal temperature

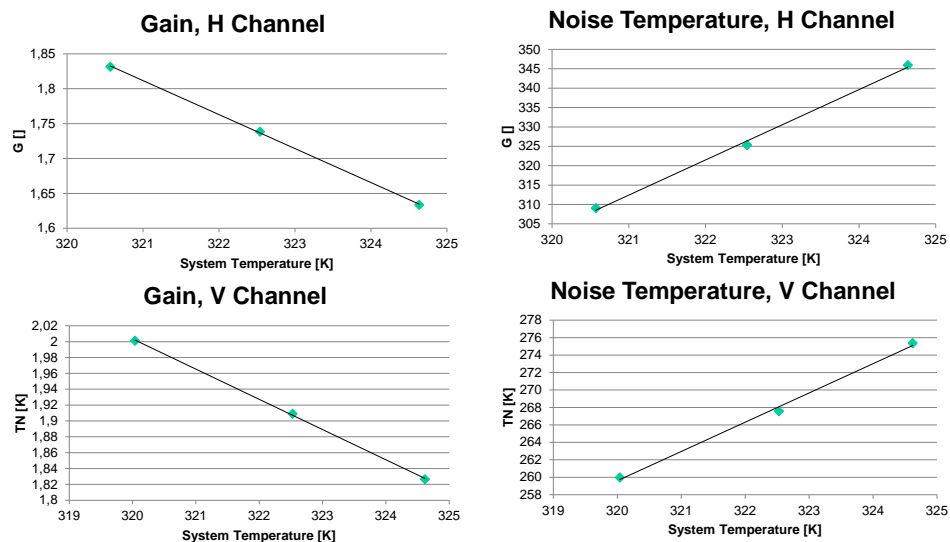


Figure 4-3 – Gain and noise temperature estimates for EMIRAD-X determined as a function of internal temperature

Almost all figures show a linear trend, and as expected the gain decreases, while the noise temperature increases for an increase in physical temperature. This is expected behaviour for most semiconductor-based amplifiers due to component physics [5]. For EMIRAD-C one point is obviously an outlier, and it is expected that this is caused by lack of temperature stability while taking the measurement. This happens if a measurement is performed before thermal equilibrium is established, and it is obviously an error by the operator.

## 4.2 Calibration of internal calibration point, Noise Diode

Following the estimation of system gain and system noise temperatures, the contribution from the Noise Diode (ND) can be estimated. For each temperature setting, an estimation is performed and the result is seen in Figure 4-4 and Figure 4-5 for EMIRAD-C and EMIRAD-X, respectively. The horizontal axis shows the physical temperature of the noise diode.

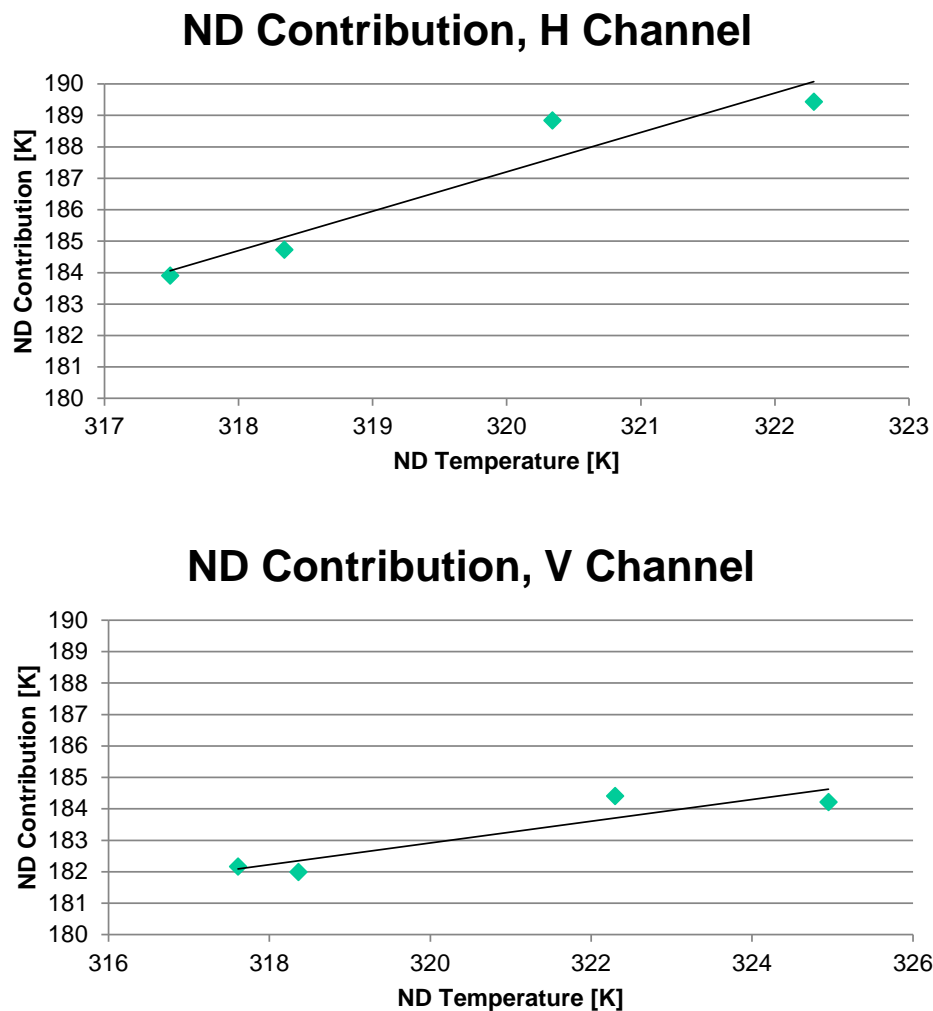
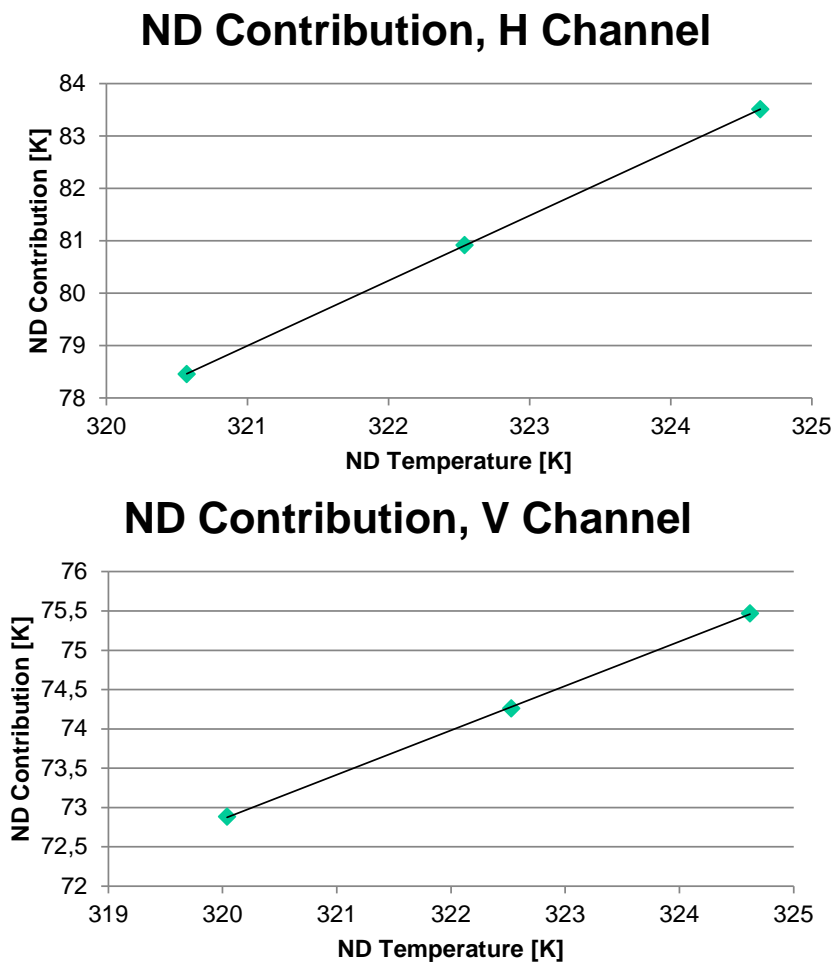


Figure 4-4 – Contribution from the noise diode to each channel for EMIRAD-C



**Figure 4-5 – Contribution from the noise diode to each channel for EMIRAD-X**

Similar to the estimates of gain and noise temperature, all estimates of the noise diode contribution show a linear trend, which is expected from component physics [4]. The outlier for EMIRAD-C represents the same data sample, which caused the outlier in the gain estimation, and it was expected, as a wrong gain estimate will compromise all following computations.

The characterization of the noise diode over the temperature range shown enables autonomous calibration of future collected measurement data without the permanent presence of a cold external calibration target, which is impractical for field experiments. The data processing application simply needs a linear model as input, providing the noise diode contribution at a given temperature along with the coefficient, describing the sensitivity to changes in the physical temperature.

The calibration target information is entered into an ASCII-file, read by the processing application on program start-up. The application features several calibration targets, and it already supports a future addition of an Active Cold Load (ACL). For EMIRAD-C the calibration target information is found in Table 4-1, and for EMIRAD-X Table 4-2 provides the figures.

Type	Brightness Temperature	Sensitivity
ML, H-Pol	Physical temperature (individually measured) 318-323 K	+1.000 K/K
ML, V-Pol		+1.000 K/K
ND, H-Pol	Input source + 188.46 K @ $T_{\text{physical}} = 321$ K	Input source + 1.252 K/K
ND, V-POI	Input source + 183.26 K @ $T_{\text{physical}} = 321$ K	Input source + 0.345 K/K

**Table 4-1 – Calibration target summary for EMIRAD-C**

Type	Brightness Temperature	Sensitivity
ML, H-Pol	Physical temperature (individually measured) 318-323 K	+1.000 K/K
ML, V-Pol		+1.000 K/K
ND, H-Pol	Input source + 81.48 K @ $T_{\text{physical}} = 323$ K	Input source + 1.242 K/K
ND, V-POI	Input source + 74.55 K @ $T_{\text{physical}} = 323$ K	Input source + 0.564 K/K

**Table 4-2 – Calibration target summary for EMIRAD-X**

The noise diode characterization not only provides a useful calibration point but also allows for estimation of system linearity as described in [4]. Comparing the estimated noise diode contribution both for a hot target and for a cold target yields this information. As the noise diode contribution is added on top of the input temperature, it should remain absolutely constant. However, if the system gain is not completely linear over the full input range, the noise diode contribution will appear to change. Table 4-3 and Table 4-4 show this comparison for EMIRAD-C and EMIRAD-X, respectively.

Channel	ND contribution Cold target	ND contribution Hot target	Non-linearity
Vertical	180.20 K	183.20 K	-1.66 %
Horizontal	183.26 K	183.89 K	-0.34 %

**Table 4-3 – Linearity validation for EMIRAD-C**

Channel	ND contribution	ND contribution	Non-linearity
	Cold target	Hot target	
Vertical	73.21 K	72.56 K	+0.89 %
Horizontal	78.72 K	78.20 K	+0.66 %

**Table 4-4 – Linearity validation for EMIRAD-X**

It is seen, that the change is very small with 1.66 % over the full range as a maximum. As the variation in gain is typically very limited, the actual impact on measurement accuracy is a few mK, which can be neglected in the total calibration budget. It is noted, that the non-linearity has a negative sign for EMIRAD-C, while it is positive for EMIRAD-X. This is very much as expected, considering the different instrument architectures. The physics will not be described further in this document, but additional examples and conclusions can be found in [4].

### 4.3 Characterization of antenna system parameters

The determination of external parameters, according to calibration steps 2 and 3 is pretty much a measurement series followed by tables of figures to feed into the processing application. Calibration step 2 requires estimation of cable losses (expressed as gain factor, G), and the setup illustrated in Figure 3-4 is applied. The results are seen in Table 4-5 for both EMIRAD-C and EMIRAD-X cables. Each cable is labelled in order to use always the same cable in the same channel for measurement campaigns. Furthermore, each cable is mounted with an individual temperature sensor in order to apply Equation

$$T_A = \frac{T_A' - (1 - G)T_P}{G} \quad (3-2) \text{ correctly.}$$

Cable	Measured S <sub>21</sub>
EMIRAD-C, H-Pol	-0,77 dB
EMIRAD-C, V-Pol	-0,81 dB
EMIRAD-X, H-Pol	-0,63 dB
EMIRAD-X, V-Pol	-0,63 dB

**Table 4-5 – Estimated cable losses for EMIRAD-C and EMIRAD-X**

The remaining parameters to be characterized all concern the antenna system. Estimation of the antenna parameters, however, is extremely difficult to do using a liquid Nitrogen cooled target, as it must be very big (bigger than the antenna aperture), and as surface reflections from the air/Nitrogen surface are difficult to account for. Hence it is decided to use a Vector Network Analyzer (VNA), Keysight Fieldfox model N9918A, which features measurements of transmission coefficients and reflection coefficients at frequencies up to 26.5 GHz. To obtain all desired parameters, an effective short circuit (metal plate fastened to the common port of the Orthomode Transducer) and a matched load (antenna view into free-space or view into a

microwave absorber in front of the antenna) must be used. The VNA and the antenna on the department rooftop measurement facility is seen in Figure 4-6.



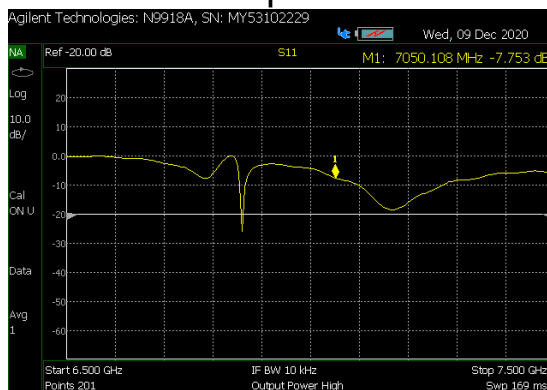
Figure 4-6 – Vector Network Analyzer (left) and antenna looking into free space (right)

For measurement of the insertion loss, the reflection is measured on the input port with the short circuit in place. The input signal will be attenuated, reflected in the short circuit, and finally it will meet the attenuation again. Hence the measurement will show 2 times the one-way insertion loss. The measurement must be performed for both polarizations in order to get the individual channel loss coefficients. Comparison of the phase between the two channels will provide 2 times the phase difference, and thus the one-way phase imbalance can be easily found. Transmission at one polarization should ideally return only in that polarization. If a cross-coupling occurs, it can be found by measuring the transmission from one antenna port to the other, while the short circuit is in place.

For estimation of the antenna system return loss, the simple reflection measurement is used, while the antenna is matched, i.e. when it looks into a free space or a microwave absorber. In this measurement the instrument reading will only contain the reflection caused by the antenna system itself.

Not all measurements are shown, but some examples are included. Figure 4-7 shows the measurement of return loss from the EMIRAD-C antenna system, and Figure 4-8 shows the cross-coupling results. For comparison, the same two measurements are shown for EMIRAD-X with the reflection and the cross-coupling in Figure 4-9 and Figure 4-10, respectively.

### Vertical polarization



### Horizontal polarization

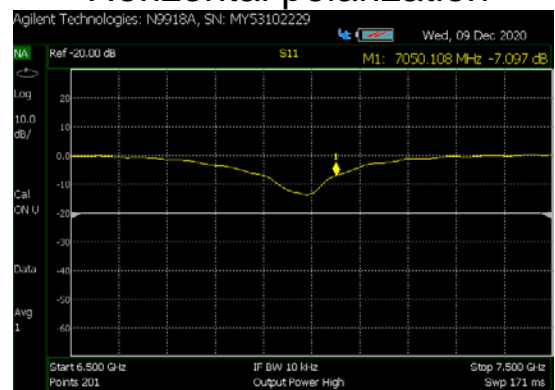


Figure 4-7 – Measurement of return loss for EMIRAD-C antenna system

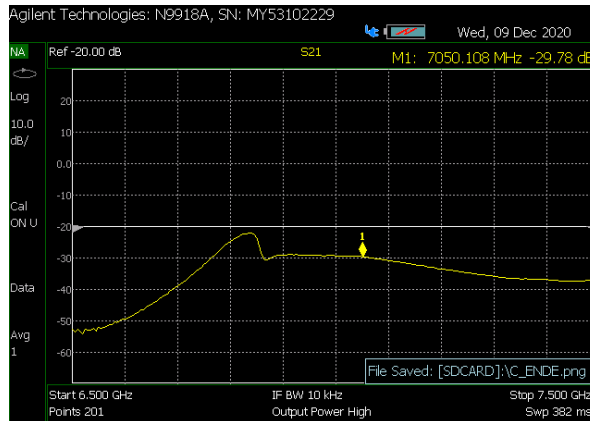
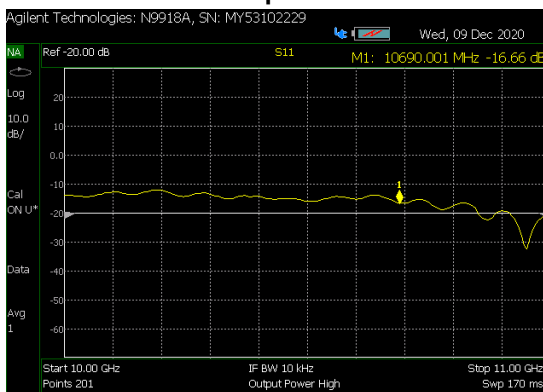


Figure 4-8 – Measurement of antenna cross coupling for EMIRAD-C

Vertical polarization



Horizontal polarization

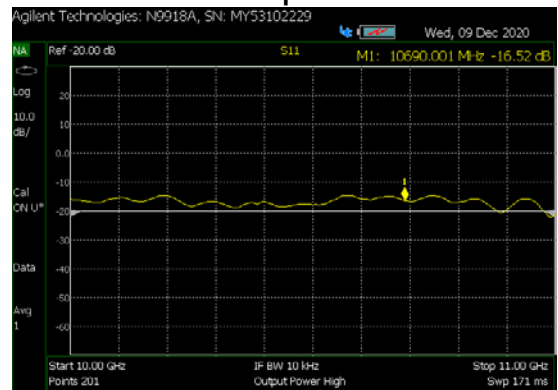


Figure 4-9 – Measurement of return loss for EMIRAD-X antenna system

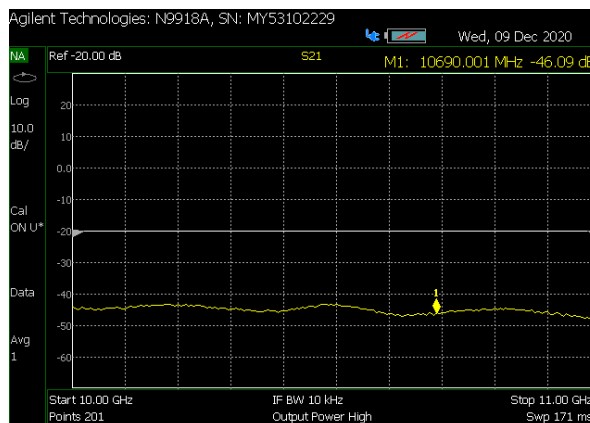


Figure 4-10 – Measurement of antenna cross coupling for EMIRAD-X

All measurement results are summarized in Table 4-6 and Table 4-7 for EMIRAD-C and EMIRAD-X, respectively, and all values are fed into the processing software in ASCII files for application in the actual data calibration process.

Parameter	Measured Value
Insertion Loss, H	-0.15 dB
Insertion Loss, V	-0.11 dB
Return Loss, H	-7.10 dB
Return Loss, V	-7.75 dB
Phase Imbalance	-167.6 degrees
Cross coupling	-29.8 dB

Table 4-6 – Estimated parameters for EMIRAD-C antenna system

Parameter	Measured Value
Insertion Loss, H	-0.30 dB
Insertion Loss, V	-0.30 dB
Return Loss, H	-16.52 dB
Return Loss, V	-16.66 dB
Phase Imbalance	N/A
Cross coupling	-46.1 dB

Table 4-7 – Estimated parameters for EMIRAD-X antenna system

#### 4.4 Long term stability

The final instrument evaluation shall address the instrument radiometric resolution and the long-term instrument drift. The expected radiometric resolution,  $\Delta T$ , is found from Equation

$$\Delta T = \frac{T_A + T_N}{\sqrt{B\tau}} \quad (4-1)$$
, where  $T_A$  is the antenna temperature,  $T_N$  the system noise temperature, and where  $B$  and  $\tau$  represent the measurement bandwidth and observation time, respectively

[4]. The equation foresees, that  $\Delta T$  plotted against  $\tau$  in a double-logarithmic coordinate system shall represent a straight line with a slope equal to -0.5 (1 over the square-root).

$$\Delta T = \frac{T_A + T_N}{\sqrt{B\tau}} \quad (4-1)$$

This expectation, however, is based upon the assumption, that the instrument is absolutely stable, and that no drift appears over time. Obviously, the assumption only holds for a certain time, and for longer and longer measurement times, the drift will become the dominant cause of uncertainty. To assess this phenomenon, a very long (several weeks) measurement series is needed, and Figure 4-11 shows EMIRAD-C and EMIRAD-X while performing this test.



Figure 4-11 – EMIRAD-C and EMIRAD-X during long term stability validation

On completion of the test, the sample-to-sample deviation is computed. Basically, this method only compares neighbouring samples, and hence it is only sensitive to periodic variations with a period, which equals the sample duration (unlike the normal standard deviation, which include all variations, regardless of the time period). Now the samples are averaged two-by-two, and the computation of the sample-to-sample deviation is repeated for the new sample period. This process is continued as long as the measurement series length allows, and the output from the computation is a plot showing the sample-to-sample deviation as a function of the observation time.

The plot will be dominated by (at least) two counter-acting effects. For small observation times, long-term drift will be negligible, and the radiometric resolution will be far the dominant

factor. However, for very long observation times, Equation  $\Delta T = \frac{T_A + T_N}{\sqrt{B\tau}} \quad (4-1)$

foresees a negligible influence from the radiometric resolution, while the sample-to sample deviation will be driven by the drift.

Plots of the sample-to-sample deviations have been generated for both radiometers, and the results are seen in Figure 4-12 and Figure 4-13 for EMIRAD-C and EMIRAD-X, respectively. EMIRAD-C has two independent receiver channels, and hence there are two independent plots. EMIRAD-X measures the two polarizations in a time multiplex, using the same physical receiver, and hence only one plot has been generated for this radiometer.

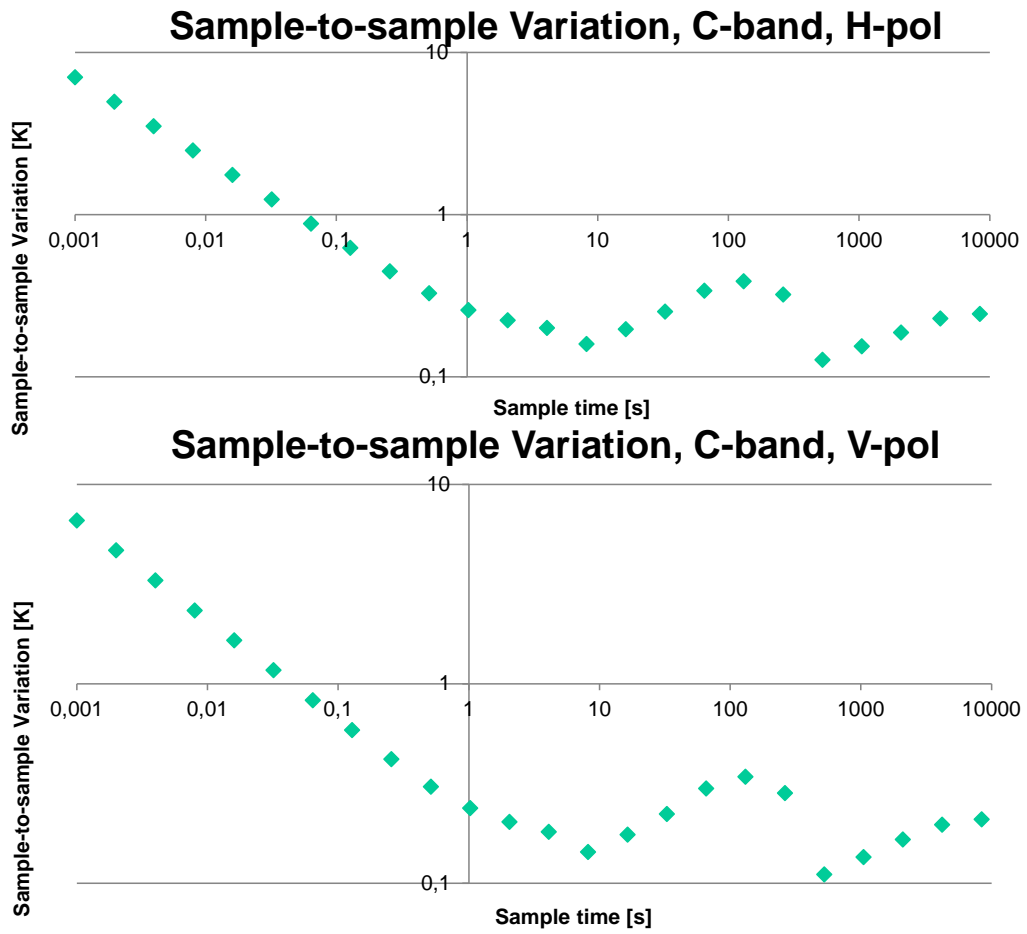
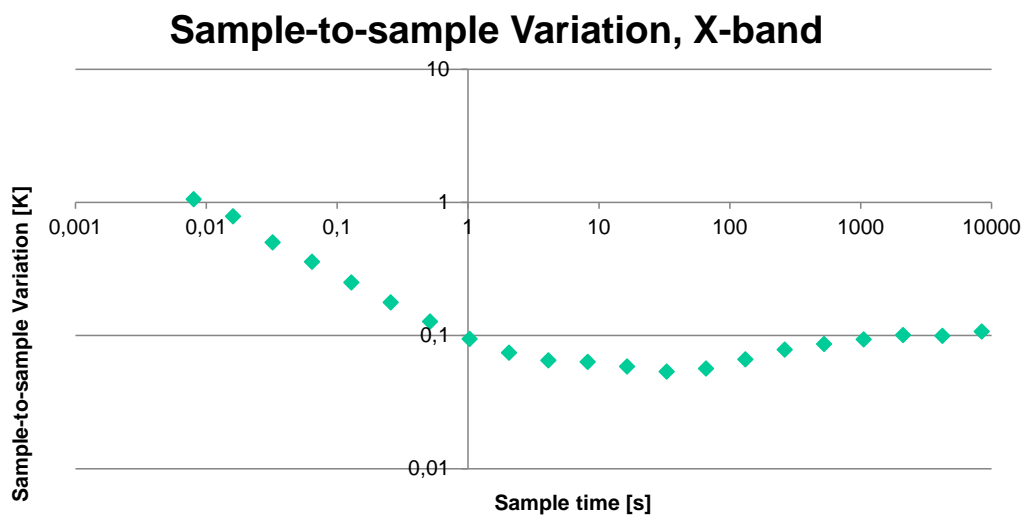


Figure 4-12 – Sample-to-sample variation, EMIRAD-C



### Figure 4-13 – Sample-to-sample variation, EMIRAD-X

Common to all three plots, it is evident that the radiometric resolution is dominant for small observations times, and a quasi-straight line with a slope equal to  $-0.5$ , resulting from  $1$  over the square-root, is observed in the left side. This confirms that drift is no issue at this time scale. All three plots also show an upward trend for very long (3 hours) observation times, confirming the duration of the observation as the overall driver for the drift. EMIRAD-C has a small peak around 200 s, corresponding to the period of (small) internal temperature variations, induced by the temperature regulation system, which has a period on the same time-scale, and which at higher ambient temperatures (around 25 degrees C and up) is known to be relatively aggressive. The phenomenon is well known from past applications of the same instrument, when it was an L-band radiometer, and it becomes much less pronounced when the instrument is operated at typical outdoor temperatures instead of in the lab. Apart from this artefact, the curves appear as expected. Furthermore, it can be seen that observation times of 10 seconds seem to yield satisfactory results in the range of 10-20 mK, and that calibration events every 5 minutes (300 seconds) would be sufficient.

## 5. PREPARATION FOR TEST CAMPAIGN

This section outlines the preparation of EMIRAD-C and EMIRAD-X for a short-term measurement campaign from a stationary platform. The purpose of the campaign is to compare the measurements of Sea Surface Temperature (SST) at microwave frequencies against SST measurements at near-optical wavelengths.

### 5.1 System setup and operation plan

Apart from the radiometers themselves, including cables and antenna system, the setup must include some sort of support structure including a shelf to allow for installation on e.g. a bridge, looking over the railing. For this particular campaign a one-shelf scaffold is used for support. The ladders are 1.95 m, and the maximum shelf level is 1.85 m with steps of approximately 30 cm downwards. For a short-term, supervised, stationary campaign it is decided to simply put the radiometers on the shelf side-by-side, fastening the instruments and the antennas to the structure using straps. A digital inclinometer is used for horn alignment and incidence angle adjustment.

A control computer, running the Graphical User Interfaces (GUI) and acting as a data storage must also be included in the system, and all units must be connected using a standard Ethernet network switch. The computer and the switch may be placed on the shelf or be remote.

The whole setup may be covered by a protective blanket if required by the weather conditions, as long as the antenna apertures are kept unobstructed. The complete instrumentation, including Ethernet switch and control/storage computer consumes approximately 550 W, and hence it is possible to use a simple 1 kW engine generator as power source for operation in remote locations, e.g. a bridge. The setup (without blanket) is seen in Figure 5-1 and Figure 5-2.



Figure 5-1 – Scaffold accommodating EMIRAD-C (left) and EMIRAD-X (right)



**Figure 5-2 – Scaffold with radiometers including control/storage computer and engine generator for autonomous operation at remote locations**

## 6. SHORT-TERM MEASUREMENT CAMPAIGN

This section describes the short-term measurement campaign that took place in order to compare microwave sea surface temperature measurements against infrared, and also presents its results.

### 6.1 Campaign site and setup

The short-term campaign took place on a small train / bike lane bridge that lies over brackish waters in Copenhagen, Denmark, on 13/1/2021. EMIRAD-C and EMIRAD-X were mounted on a scaffold, as described on paragraph 5.1. The infrared radiometer ISAR was mounted on the bridge bars right next to the microwave radiometers. Figure 6-1 – Short-term microwave/infrared radiometer measurement campaign setup Figure 6-1 shows the full setup of the campaign.



Figure 6-1 – Short-term microwave/infrared radiometer measurement campaign setup

### 6.2 Brief description of the infrared radiometer

The infrared radiometer used for the campaign is the ISAR-019, created by the University of Southampton and owned by DMI. ISAR measures radiance at the spectral waveband 9.8-11.5  $\mu\text{m}$ . More information about the instrument, as well as the ISAR project in general, can be found at [www.isar.org.uk](http://www.isar.org.uk) and [www.ships4sst.org](http://www.ships4sst.org).

### 6.3 Qualitative description of experiment conditions

During the experiment, there was low wind combined with high humidity and, on a couple of occasions, there was light rain and snow. The ISAR is designed to stop measurements when it detects rain through a connected sensor so the occasional rain and snow resulted in a small gap in infrared measurements. The air temperature was also generally cold, not reaching above than 1-2  $^{\circ}\text{C}$ .

## 6.4 Results

### 6.4.1 ISAR results

The sea surface temperatures measured by ISAR show small fluctuations, as seen on Figure 6-2.

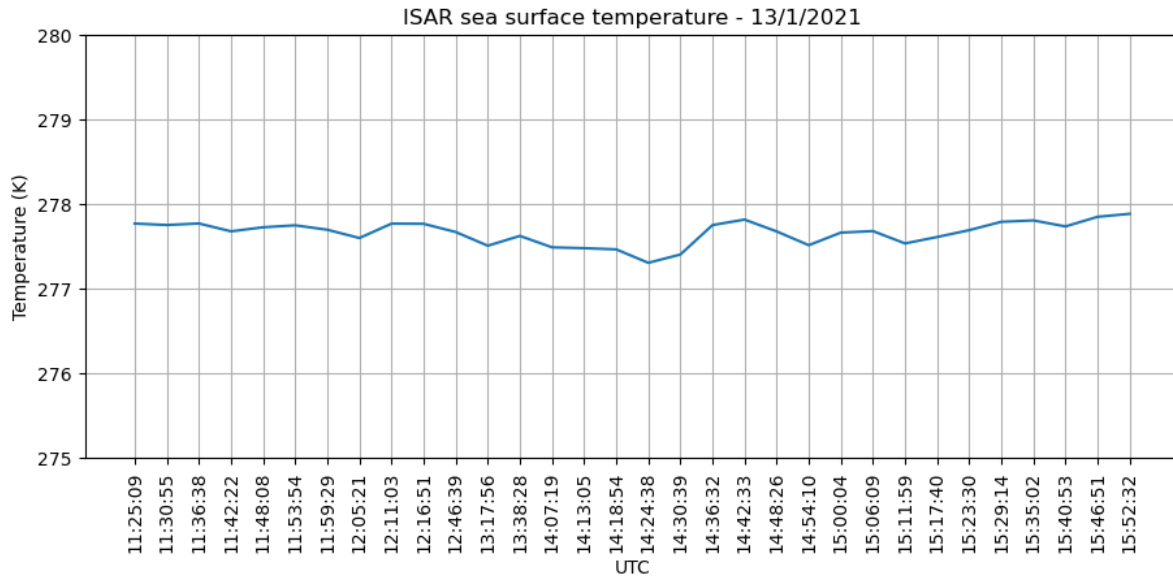


Figure 6-2 – ISAR sea surface temperature on 13/1/2021

### 6.4.2 MW results

Figures Figure 6-3 and Figure 6-4 show the measured brightness temperatures for EMIRAD-C and EMIRAD-X respectively.

During the first hour of the experiment, EMIRAD-C's vertical polarization measurements show a slope that converges to the average brightness temperature measured throughout the rest of the experiment, due to temperature regulation of the receivers. EMIRAD-X does not show the same slope in the beginning because its temperature regulation time is shorter. Large fluctuations in the EMIRAD-C horizontal polarization channel are seen in the measurements throughout the first four hours of the experiment. The reason for this is not known, but the calibration data throughout the experiment do not show any irregularities, which points towards external factors. We suspect that this is possibly due to Radio Frequency Interference entering the antenna. A repetition of the experiment at another site, where repeated sky observations will be conducted, could probably give more information about this variability. During the experiment, the sky was measured only once for a 5 minutes interval, observing an average sky brightness temperature of 16.37 K and 17.75 K (V-pol and H-pol respectively) for C-band, and 26.50 K and 27.09 K (V-pol and H-pol respectively) for X-band.

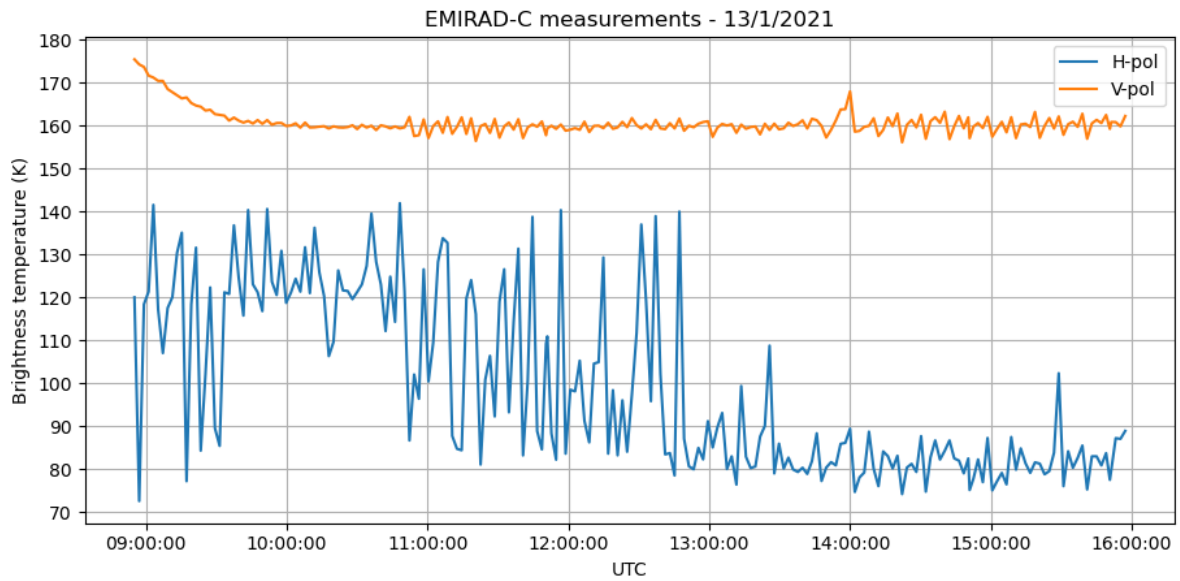


Figure 6-3 – EMIRAD-C brightness temperature measurements on 13/1/2021

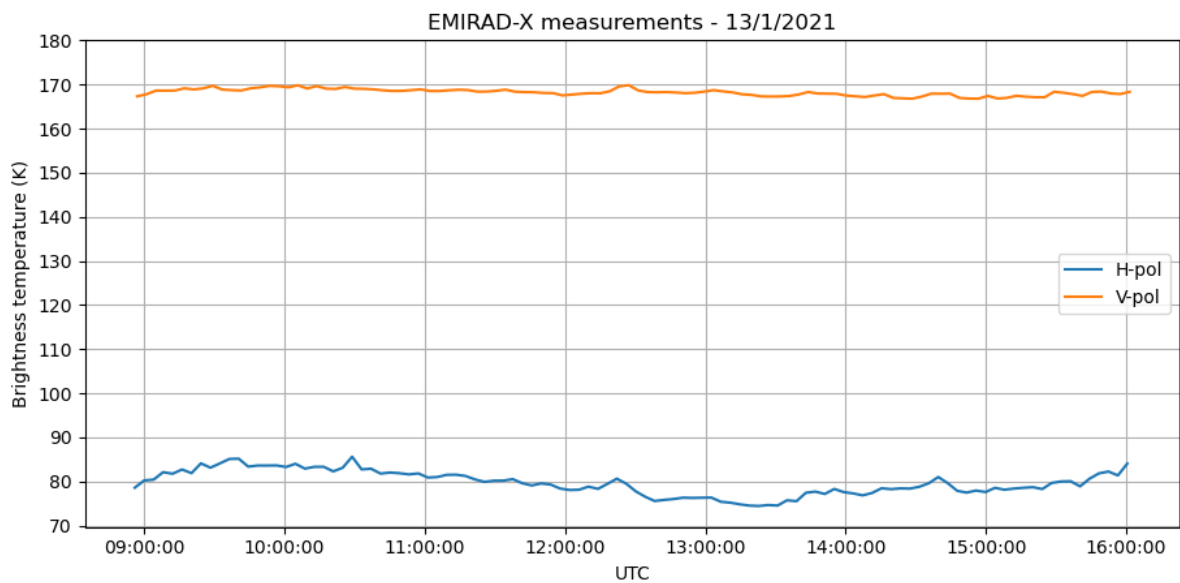


Figure 6-4 – EMIRAD-X brightness temperature measurements on 13/1/2021

### 6.4.3 Intercomparison

In order to derive the physical temperatures from the microwave measurements, we applied a 5-term linear regression model, with the ISAR SSTs as the independent variable. Temperatures from both instruments are seen on Figure 6-5, and the regression coefficients on Table 6-1. It is seen that the estimated SSTs are dominated by observations from the X-

band V-pol channel. Under normal conditions with cold water, retrievals should be based primarily on information from the C-band observations.

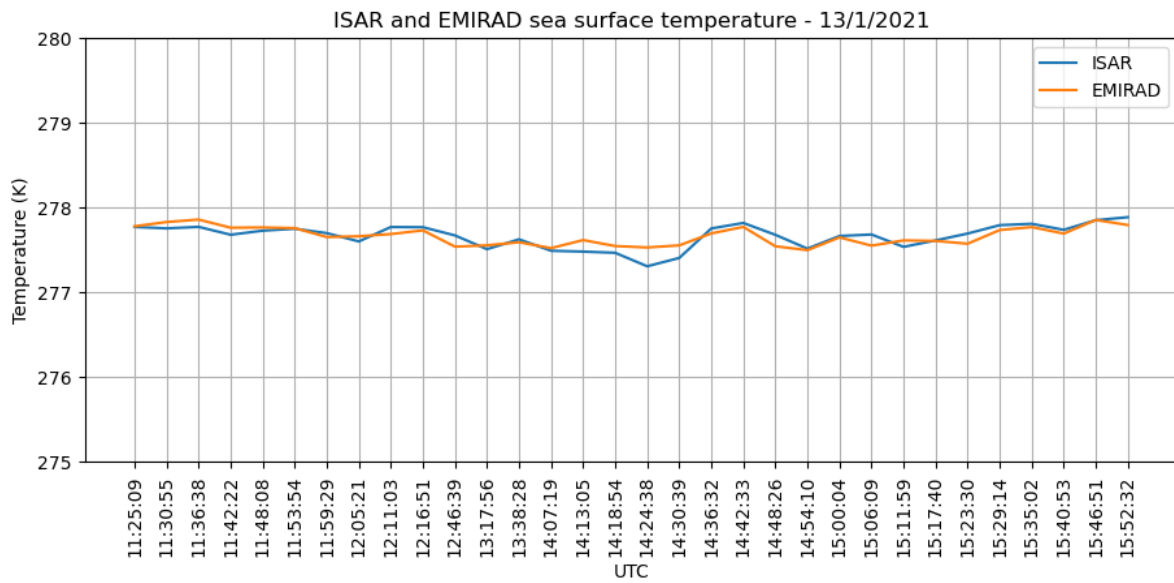


Figure 6-5 – Temperature comparison between ISAR and EMIRAD

Intercept	C-band VP coeff.	C-band HP coeff.	X-band VP coeff.	X-band HP coeff.
250.8108576454614	-0.01528234	-0.00192514	0.16244991	0.02830327

Table 6-1 – Regression coefficients for the calculation of EMIRAD physical temperatures

## 7. SUMMARY AND CONCLUSIONS

This document outlines the refurbishment of two outdated radiometers to measure brightness temperatures at C-band and X-band at two orthogonal polarizations, with at least the C-band sensor able to provide the full Stokes vector. The refurbishment includes preparation of full functional antenna systems for future campaign use, and the complete hardware is seen in Figure 7-1.



Figure 7-1 – The full hardware for measurements of brightness temperatures at C-band (upper row photographs) and X-band (lower row photographs)

### 7.1 Main characteristics

For the C-band radiometer, named EMIRAD-C, the main properties are:

- Fully polarimetric, i.e. measures all four Stokes parameters in parallel
- 2 physical antenna polarizations, dual polarized antenna
- Frequency band (-3 dB): 7.0365 – 7.0635 GHz
- Frequency band (-20 dB): 7.025 – 7.075 GHz
- Features well characterized internal noise diode for autonomous calibration
- $\Delta T = 0.25$  K for integration time  $\tau = 1$  s

For the X-band radiometer, named EMIRAD-X, the main properties are:

- Dual polarimetric, i.e. measures 1<sup>st</sup> and 2<sup>nd</sup> Stokes parameters (time multiplex)
- 2 physical antenna polarizations, dual polarized antenna
- Frequency band (-3 dB): 10.64 – 10.74 GHz
- Frequency band (-10 dB): 10.59 – 10.79 GHz
- Features well characterized internal noise diode for autonomous calibration
- $\Delta T = 0.1$  K for integration time  $\tau = 1$  s

Common properties of the instruments are:

- Fully characterized
- Fully flexible calibration scheme (programmable via ASCII input file)
- Graphical user interface
- Control and data storage via standard Ethernet protocols
- 4-step calibration scheme included in software package
- Data product output in easy-to-read ASCII file

## 7.2 Conclusions

Two radiometers for C-band and X-band Earth observations have been prepared for a short-term measurement campaign as well as for future campaigns, possibly on a moving platform. Both instruments have been tested and validated in the laboratory, and all essential parameters have been characterized, i.e. gain, noise temperature, radiometric resolution and long-term stability. Furthermore, all relevant calibration input parameters have been measured and characterized, and software applying the parameters is provided for easy data processing.

Both instruments fully live up to the expectations, and they are considered ready for measurement campaigns in the present stage. Possibilities for future further development exist, and new components have all been chosen, so that they can be used in further upgraded systems, e.g. systems with enhanced bandwidth, if the digital subsystems are upgraded in the future.

Both radiometers come fully equipped with dual polarized antenna systems, and they both measure dual polarized at horizontal and vertical polarizations. Furthermore, the C-band radiometer provides 3<sup>rd</sup> and 4<sup>th</sup> Stokes parameters for fully polarimetric data analysis as well as true corrections for all measurement artefacts. The sensors feature fully automatic calibration for easy operation and fast data delivery.

A setup has been prepared for stationary installation of the two radiometers on a bridge. The setup accommodates sensors as well and antennas, and it operates fully autonomously during measurements.

An experiment was conducted to compare the sea surface temperatures of the microwave radiometers against infrared radiometer measurements. This was the first time such an IR-MW radiometer inter-comparison experiment has been performed, and the outcome provided valuable information into future inter-comparison campaigns. The experiences and lessons learned have also been included in the first version of a deployment protocols for MW radiometers [6].

The results show increased noise on the C-band MW radiometer observations, probably due to external factors like RFI or other factors. A good agreement can be obtained between the IR and PMW observed SSTs, as seen in Figure 6-5. However, the best agreement is obtained with information from the X-band observations. This was not expected due to the lower sensitivity of the X-band observations for cold waters, compared to the C-band sensitivity. Detailed investigations are ongoing to assess the sources of the observed C-band variability and it is recommended to repeat the static experiment at another site, to rule out possible RFI effects. In addition, a repeated experiment could also increase the temporal sampling of the sky measurements to determine the sky variability over time in C-band and X-band.

## **8. REFERENCES**

- [1] "Designer Notes for Microwave Antennas", Richard C. Johnson, Artech House, 1991
- [2] "The Airborne EMIRAD L-Band Radiometer System", Søbjaerg, S.S., et al., IEEE Proceedings of IGARSS 2013, 2013
- [3] "Performance assessment of an LNA used as active cold load", Søbjaerg, S.S., et al., IEEE Proceedings of IGARSS 2015, 2015
- [4] "Microwave Radiometer Systems: Design and Analysis", Niels Skou and David M. LeVine, Artech House, 2006
- [5] "Microwave Engineering Passive Circuits", Rizzi, P. A., Prentice Hall, Englewood Cliffs
- [6] "Characterisation Report", Høyer, J. L., Skarpalezos, S. & Søbjaerg, S. S., FRM4SST report: FRM4SST-PRD-DMI-001.